Research Square

Preprints are preliminary reports that have not undergone peer review.
They should not be considered conclusive, used to inform clinical practice,
or referenced by the media as validated information.

Thermal–Hydraulic Performance of a Shell-and-Tube Heat Exchanger Using Oil-Based Nanofluids: A Two-Phase CFD Modeling Approach

Mohamed Rashad Ali

m.rashad@eng.cu.edu.eg

Cairo University

Mahmoud A. Fouad

Cairo University

Ahmed Abu-Zaid

Cairo University

Ahmed M. Hafez

Cairo University

Research Article

Keywords: Oil-based nanofluids, Computational fluid dynamics, Overall heat transfer coefficient, Slip velocity, Optimum volume fraction, Heat transfer enhancement

Posted Date: November 18th, 2026

DOI: https://doi.org/10.21203/rs.3.rs-11569409/v1

License: This work is licensed under a Creative Commons Attribution 4.0 International License.
Read Full License

Additional Declarations: No competing interests reported.

Thermal–Hydraulic Performance of a Shell-and-Tube Heat Exchanger Using Oil-Based Nanofluids: A Two-Phase CFD Modeling Approach

Mohamed Rashad Ali[a,*], Mahmoud A. Fouad[a], Ahmed Abu-Zaid[a], Ahmed M. Hafez[a]

[a] Mechanical Power Engineering Department, Faculty of Engineering, Cairo University, Giza 12613, Giza, Egypt.

Abstract

Nanofluids are promising for improving heat transfer in oil-based thermal systems, but their predicted behavior in shell-and-tube heat exchangers depends on how particles and base fluid are represented numerically. This study evaluates the thermal-hydraulic performance of oil-based nanofluids using single-phase (SP) and two-phase (TP) CFD formulations. Both models were validated against published experimental data for Al_2O_3/water nanofluids and reproduced the measured trends, with mean absolute percentage errors of 7.14% to 15.02% for TP and 9.37% to 16.47% for SP. Cu, CuO, and TiO_2 nanoparticles dispersed in Therminol LT were then examined at volume fractions of 1, 2, 3, 5, and 6%. SP predicted overall heat transfer coefficients up to about 9.5% higher than TP. For Cu nanofluids, the maximum improvement over pure oil was about 10.7% with SP and about 3.8% with TP, while pressure drop was nearly identical for both. TP results showed very low slip velocities, indicating strong phase coupling and negligible particle redistribution. The thermal differences are attributed mainly to phase representation and local thermophysical-property treatment. Cu performed best, followed by CuO and TiO_2. The optimum concentration was about 5 vol.% with SP and about 3 vol.% with TP. The formulation strongly influenced predicted heat transfer and optimum concentration, but had limited effect on pressure drop and particle ranking.

.

Keywords: Oil-based nanofluids; Computational fluid dynamics; Overall heat transfer coefficient; Slip velocity; Optimum volume fraction; Heat transfer enhancement.

* **Email address of corresponding author:** m.rashad@eng.cu.edu.eg (Mohamed Rashad Ali).
-Email addresses of other authors: dr.mahmoud.fouad@gmail.com (Mahmoud A. Fouad), ahmedabouzaid@eng.cu.edu.eg (Ahmed Abu-Zaid), ahafez@cu.edu.eg (Ahmed M. Hafez).

Nomenclature

Abbreviation	
CFD	Computational Fluid Dynamics
LMTD	Log Mean Temperature Difference
PEC	Performance evaluation criterion
STHE	Shell-and-Tube Heat Exchanger
TP	Two-Phase
SP	Single-Phase
English	
A	Heat transfer area, m^2
C_p	Specific heat capacity, J/kg.K
d	Diameter, m
f	Friction factor
h	Heat transfer coefficient, $W/m^2.K$
k	Thermal conductivity, W/m.K
K_B	Boltzmann constant
Pe	Peclet number
Pr	Prandtl number
Q	Heat transfer rate, kW
Re	Reynolds number
T	Temperature, K
U	Overall heat transfer coefficient, $W/m^2.K$
V_B	Brownian velocity of nanoparticles, m/s
$\dot{m}$	Mass flow rate, kg/s
ΔP	Pressure drop, kPa
ΔT_{lmtd}	Log mean temperature difference, K
Greek	
δ	Distance between the centers of particles, m
φ	Volume fraction, %
μ	Dynamic viscosity, $kg/m.s$
ρ	Density, kg/m^3
Sub/Superscripts	
c	Cold fluid
f	Base fluid
h	Hot fluid
in	Inlet
m	Mixture
nf	Nanofluid
out	Outlet
p	Nanoparticles
s	Shell side
t	Tube side

1. Introduction

Shell-and-tube heat exchangers (STHEs) are among the most widely utilized thermal systems in industrial applications because of their simplicity, reliability, and ability to operate under high-pressure and high-temperature conditions [1]. They are extensively employed in thermal power plants, petrochemical facilities, heating, ventilation, and air-conditioning (HVAC) systems, thermal energy recovery units, and industrial process engineering. Improving the thermal efficiency of STHEs remains an important engineering objective because heat exchanger performance directly affects energy consumption, operational costs, and overall system effectiveness [2]. However, conventional heat transfer fluids, such as water, ethylene glycol, and thermal oils, generally possess relatively low thermal conductivity, which limits their heat transfer capability. To overcome this limitation, nanofluids have emerged as a promising approach for enhancing heat transfer performance [3,4].

Nanofluids are produced by dispersing nanoparticles, typically smaller than 100 nm, into conventional base fluids [5]. Numerous studies have demonstrated that incorporating nanoparticles can improve the thermal conductivity of the working fluid and enhance convective heat transfer performance under appropriate operating conditions [6–8]. Nevertheless, these thermal benefits may be accompanied by increased viscosity, pressure drop, and pumping power requirements [9]. Consequently, evaluating nanofluid performance requires simultaneous consideration of thermal enhancement and the associated hydraulic penalties to determine whether the resulting improvement is beneficial from an engineering perspective [10,11]. Computational Fluid Dynamics (CFD) has therefore become an important tool for investigating nanofluid flow, heat transfer mechanisms, and the influence of operating parameters on thermal system performance [12,13].

Two principal modeling approaches are commonly employed in CFD simulations of nanofluids: the single-phase (SP) approach and the two-phase (TP) approach [14]. In the SP formulation, the nanofluid is treated as a homogeneous fluid whose effective thermophysical properties account for the presence of nanoparticles. This approach offers computational efficiency and numerical simplicity, making it widely used in engineering simulations [15,16]. However, it does not explicitly resolve the separate transport behavior of the nanoparticle and base-fluid phases. Consequently, particle migration, relative motion between phases, and other local interphase transport effects cannot be directly represented in the same manner as in multiphase formulations.

In contrast, the TP approach represents the base fluid and dispersed nanoparticles as distinct phases and accounts for their interactions through appropriate multiphase transport equations. Depending on the selected formulation, these models can incorporate interphase momentum and heat transfer, as well as relative motion between the phases. Common multiphase approaches include the Eulerian–Eulerian model, the Eulerian–Lagrangian approach, commonly implemented through the Discrete Phase Model (DPM), and the mixture model [16–19]. The mixture model provides a useful compromise between computational cost and physical representation by accounting for interphase slip and solving mixture transport equations, subject to the assumptions of the formulation [16–19]. Therefore, a TP formulation can provide additional insight into the influence of nanoparticle transport and phase interactions on nanofluid flow and heat transfer, particularly when nanoparticle concentration and material properties vary. Nevertheless, its suitability

depends on the physical assumptions, constitutive relations, numerical implementation, and validation of the model for the specific application.

Previous investigations have examined different CFD formulations for predicting nanofluid heat transfer. Akbari et al. [15], for example, investigated laminar mixed convection of Al_2O_3–water nanofluids using single-phase and several two-phase models. Their results indicated that the predicted thermal fields and convective heat transfer coefficients depended on the selected formulation, with the two-phase models providing closer agreement with experimental data for the conditions considered. Further comparative investigations have also examined the prediction of nanofluid heat transfer under different flow conditions and modeling assumptions [16–18,20,21]. These studies demonstrate the importance of selecting an appropriate CFD formulation when evaluating nanofluid behavior. However, the accuracy and applicability of any model must be assessed in relation to the particular fluid system, flow regime, geometry, and available experimental evidence.

Despite the extensive research on nanofluids, much of the literature on heat transfer enhancement in shell-and-tube heat exchangers has concentrated on water-based nanofluids [22,23]. For example, Farajollahi et al. [24] experimentally investigated the heat transfer characteristics of γ-Al_2O_3–water and TiO_2–water nanofluids in a shell-and-tube heat exchanger, examining the effects of nanoparticle type, concentration, and flow conditions. Although such studies have contributed significantly to understanding the thermal behavior of water-based nanofluids, their findings cannot necessarily be transferred directly to oil-based systems because of differences in thermophysical properties, including thermal conductivity, viscosity, density, and specific heat capacity.

Oil-based nanofluids present an important research opportunity because thermal oils are used in industrial applications requiring heat transfer at elevated temperatures. However, their thermal–hydraulic behavior can differ substantially from that of water-based nanofluids. The addition of nanoparticles may alter the effective thermal conductivity and viscosity of the oil, thereby influencing convective heat transfer, pressure drop, and pumping requirements. These effects depend on both the nanoparticle material and its concentration. In particular, a systematic investigation of oil-based nanofluids containing copper (Cu), copper oxide (CuO), and titanium dioxide (TiO_2) nanoparticles is needed to establish how these materials affect heat transfer enhancement and the associated hydraulic penalties in shell-and-tube heat exchangers.

A comprehensive evaluation of these nanofluids also requires an appropriate representation of nanoparticle transport. The TP CFD approach offers a means of investigating the behavior of the dispersed nanoparticles and their interaction with the base fluid rather than treating the nanofluid solely as a homogeneous medium. This is particularly relevant when assessing the effects of nanoparticle type and concentration on the local flow field and heat transfer characteristics. Moreover, evaluating thermal performance independently of pressure drop may lead to misleading conclusions regarding the practical benefits of nanoparticle addition. Therefore, heat transfer enhancement, pressure drop, and overall thermal–hydraulic performance should be considered together when identifying suitable nanoparticle concentrations for engineering applications.

For numerical reliability, CFD predictions should be assessed against appropriate experimental and analytical benchmarks. Experimental data provide a basis for evaluating

the model's ability to reproduce measured thermal behavior, while established heat transfer correlations and conventional thermal-resistance relations provide complementary checks on the predicted heat transfer coefficients and overall thermal performance [1,25]. In the present study, the numerical methodology is validated against published experimental benchmark data reported by Farajollahi et al. [24] and further assessed using analytical calculations based on the Gnielinski correlation and conventional thermal-resistance relations [1,25].

Based on the aforementioned considerations, further investigation is needed into the thermal–hydraulic behavior of oil-based nanofluids containing different nanoparticle materials, particularly Cu, CuO, and TiO_2, in shell-and-tube heat exchangers. In this context, employing a two-phase (TP) CFD model is important because it represents the nanoparticle and base-fluid phases separately and accounts for their interactions, providing additional insight into nanoparticle transport and its influence on flow and heat transfer behavior. Accordingly, the present study employs a TP CFD model to investigate the thermal–hydraulic performance of Cu-, CuO-, and TiO_2-based oil nanofluids over a range of nanoparticle concentrations. Particular attention is given to the effects of nanoparticle type and concentration on heat transfer enhancement, pressure drop, and overall thermal–hydraulic performance, with the aim of identifying the optimum nanoparticle concentration and operating conditions. Through this investigation, the study seeks to contribute to a better understanding of oil-based nanofluids in shell-and-tube heat exchangers and provide practical insights into their application for thermal performance enhancement and engineering optimization.

2. Numerical Methodology

2.1. Physical Model Description

The present study investigates turbulent nanofluid flow and heat transfer in a shell-and-tube heat exchanger using both single-phase (SP) and two-phase (TP) CFD formulations. The shell-and-tube heat exchanger geometry adopted in the present study was based on the experimental configuration reported by Farajollahi [24]. The heat exchanger consists of sixteen tubes arranged inside a cylindrical shell. The tube inner diameter is 4.1 mm, the tube length is 815 mm, and the shell diameter is 55.6 mm. Segmental baffles with a spacing of 50.8 mm are installed along the shell side to enhance turbulence and heat transfer performance as shown in Figure 1. The heat exchanger operates with hot oil-based nanofluid flowing through the tube side, while cold water circulates through the shell side in a counter-flow arrangement. The inlet and outlet manifolds were excluded from the computational domain because the present investigation focused on the active heat-transfer region of the shell-and-tube heat exchanger. Three nanoparticle materials with diameter 50 nm were investigated: copper (Cu), copper oxide (CuO), and titanium dioxide (TiO_2). The nanoparticles were dispersed within the hot oil base fluid at different volume fractions in order to evaluate their influence on thermal enhancement, pressure drop, and thermal–hydraulic performance. A three-dimensional computational domain was developed in order to capture conjugate heat transfer behavior and local thermal–hydraulic characteristics within the exchanger.

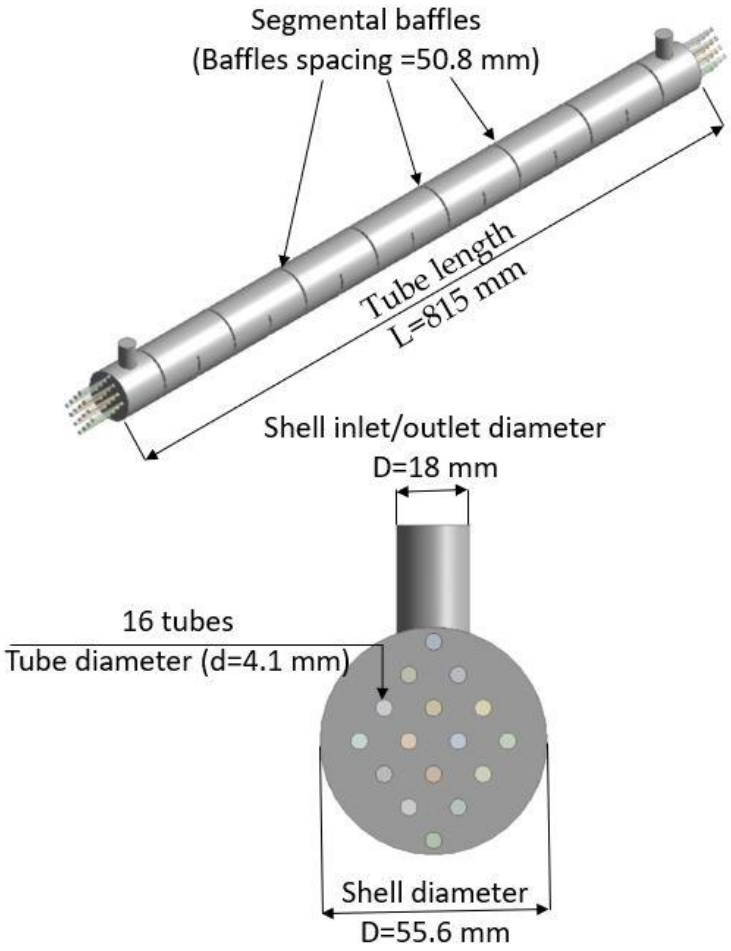


Figure 1: 3-D view and cross section view of the shell and tube heat exchanger.

2.2. Single-Phase CFD Formulation

In the single-phase formulation, the nanofluid was modeled as a homogeneous fluid with effective thermophysical properties. The nanoparticles and base fluid were assumed to move with identical velocity and temperature fields without relative slip or concentration variation. The governing equations for continuity, momentum, and energy conservation were solved for the effective nanofluid properties, expressed in Eqs. (1–3), respectively [26,27].

$$\nabla \cdot (\rho_{nf} \vec{V}) = 0 \tag{1}$$

$$\nabla \cdot (\rho_{nf} \vec{V}\vec{V}) = -\nabla P + \nabla \cdot (\mu_{nf} (\nabla \vec{V} + (\nabla \vec{V}_m)^T)) \tag{2}$$

$$\rho_{nf} C_{p,nf} (\vec{V} \cdot \nabla T) = \nabla \cdot (k_{nf} \nabla T) \tag{3}$$

where ρ_{nf} is the effective nano fluid density (kg/m³), μ_{nf} is the effective viscosity of the nanofluid (Pa·s), $C_{p,nf}$ is the nano fluid specific heat capacity (J/kg·K), k_{nf} is the nano fluid thermal conductivity (W/m·K). The thermophysical properties of the nanofluid were evaluated as functions of nanoparticle volume fraction using effective property correlations adopted in the literature [28]. The effective density of the nanofluid was calculated as:

$$\rho_{nf} = \rho_f * (1 - \varphi) + \rho_p * \varphi \tag{4}$$

where ϕ is the nanoparticle volume fraction, ρ_f is the base fluid density (kg/m³), ρ_p is the nanoparticle density (kg/m³) [28]. The effective specific heat capacity was determined from:

$$C_{p,nf} = \frac{\rho_f * (1-\varphi)}{\rho_{nf}} * C_{p,f} + \frac{\rho_p * \varphi}{\rho_{nf}} * C_{p,p} \quad (5)$$

where $C_{p,f}$ is the base fluid specific heat capacity (J/kg·K), $C_{p,p}$ is the nanoparticle specific heat capacity (J/kg·K). The thermal conductivity of the nanofluid (K_{nf}) is obtained through Eq. (6) as proposed by Yu and Choi [29]. The interfacial nanolayer parameter was set to β=0.1, following the model proposed by Yu and Choi [29]. This value represents a nanolayer thickness equal to approximately 10% of the nanoparticle radius. This approach has been further supported by experimental observations, for example, by Xie et al. [30].

$$k_{nf} = k_f * \frac{k_p + 2 * k_f + 2 * (k_p - k_f) * (1+\beta)^3 * \varphi}{k_p + 2 * k_f - (k_p - k_f) * (1+\beta)^3 * \varphi} \quad (6)$$

where k_f is the base fluid thermal conductivity (W/m·K), k_p is the nanoparticle thermal conductivity (W/m·K). The nanofluids' effective viscosity is computed according to the model proposed by Masoumi et al. [31] as expressed in Eqs. (7–11). The Masoumi viscosity model accounts for the apparent viscosity contribution arising from nanoparticle Brownian motion and interparticle interactions, where apparent viscosity represents the additional resistance of the nanofluid to deformation and flow beyond the intrinsic viscous resistance of the base fluid. This additional contribution arises from particle-induced momentum transport associated with Brownian motion and interparticle interactions. The correction factor C is evaluated using empirical constants determined from experimental nanofluid data.

$$\mu_{nf} = \mu_{bf} + \mu_{app} \quad (7)$$

where μ_{bf} is the viscosity of the basal fluid (Pa·s), and μ_{app} is the apparent viscosity contribution due to nanoparticles (Pa·s), calculated as follows:

$$\mu_{app} = \frac{\rho_{np} * V_B * {d_{np}}^2}{72C * \delta} \quad (8)$$

$$V_B = \frac{1}{d_p}\left(\frac{18 * K_B * T}{\pi * \rho_{np} * d_{np}}\right)^{\frac{1}{2}} \quad (9)$$

$$\delta = \left(\frac{\pi}{6\varphi}\right)^{\frac{1}{3}} * d_{np} \quad (10)$$

$$C = \frac{1}{\mu_{bf}}\left[\left(c_1 * d_{np} + c_2\right) * \varphi + \left(c_3 * d_{np} + c_4\right)\right] \quad (11)$$

where d_{np} is the nanoparticle diameter (nm), assumed to be 50 nm in this study, V_B is the nanoparticles' Brownian velocity. (m/s), K_B is the Boltzmann constant (1.38065×10^{-23} J/K), T is the absolute temperature (K), δ is the distance between the centers of particles (m), C is an empirical correction factor (dimensionless), obtained from regression with experimental data, The numbers c1, c2, c3, and c4 are empirical constants provided by Masoumi et al. [31] after validating his model with different nanofluids ($c_1 = -1.133\times10^{-6}$, $c_2 = -2.771\times10^{-6}$, $c_3 = 9.0\times10^{-8}$, and $c_4 = -3.93\times10^{-7}$).

2.3. Two-Phase Mixture Model Formulation

Several multiphase approaches are available for CFD simulation of nanofluids, including the Eulerian model, the Mixture model, the Volume of Fluid (VOF) model, and the Eulerian–Lagrangian (Discrete Phase Model) [32]. In the present study, the Mixture model available in ANSYS Fluent was adopted. The Mixture model treats the phases as interpenetrating continua and solves the conservation equations for the mixture together with a transport equation for the dispersed nanoparticle phase. In addition, the formulation incorporates the relative motion between the nanoparticles and the base fluid through the drift-velocity concept, providing a more physically representative description of nanoparticle transport than the homogeneous single-phase formulation [32]. The continuity equation for the mixture is expressed as:

$$\nabla \cdot (\rho_m \vec{V}_m) = 0 \tag{12}$$

where ρ_m and $\vec{V}_m$ are the mixture density and mass-averaged mixture velocity, respectively. The momentum equation is written as:

$$\nabla \cdot (\rho_m \vec{V}_m \vec{V}_m) = -\nabla P + \nabla \cdot (\mu_m (\nabla \vec{V}_m + (\nabla \vec{V}_m)^T)) + \nabla \cdot \left(\sum_k \alpha_k \rho_k \vec{V}_{dr,k} \vec{V}_{dr,k} \right) \tag{13}$$

where P is the pressure, μ_m is the mixture dynamic viscosity, $\alpha_k$is the phase volume fraction of phase k, and $\vec{V}_{dr,k}$is the drift velocity of phase k relative to the mixture velocity. The effective dynamic viscosity of the nanofluid was evaluated using the Masoumi model and implemented in ANSYS Fluent through a user-defined function (UDF). This approach was adopted because nanofluid viscosity cannot generally be represented adequately by a simple phase-averaging formulation. Consequently, several literature-based models, including those proposed by Einstein, Brinkman, Krieger–Dougherty, Wang, Corcione, and Masoumi, have been developed to provide a more physically representative prediction of nanofluid viscosity. In the present study, the Masoumi model was implemented through a UDF. The UDF evaluates the effective viscosity locally in every computational cell as a function of the local temperature and the local nanoparticle volume fraction. Therefore, the viscosity is updated iteratively during the CFD solution according to the local thermophysical conditions instead of being treated as a uniform property throughout the computational domain. The energy equation for the mixture is expressed as:

$$\nabla \cdot (\sum_k \alpha_k \rho_k \vec{V}_k h_k) = \nabla \cdot (k_{eff} \nabla T) \tag{14}$$

where α_K is the volume fraction of phase k, ρ_K is the density of phase k, $\vec{V}_k$ is the velocity of phase k h_k is the specific enthalpy of phase k, k_{eff} is the effective thermal conductivity of the mixture, and T is the mixture temperature. The effective thermal conductivity of the nanofluid was implemented through a user-defined function (UDF) based on the Yu and Choi model [29]. This approach was adopted because the thermal conductivity of nanofluids is commonly evaluated using experimentally validated effective-medium correlations rather than a general phase-averaging formulation. Numerous studies have demonstrated that the effective thermal conductivity of nanofluids depends on several factors, including nanoparticle volume fraction, particle shape, particle size, and the thermal conductivities of

both the nanoparticles and the base fluid. Consequently, correlations and other effective-medium models have been extensively employed to predict the thermal conductivity of nanofluids and have become the standard approach in the literature. Therefore, the Yu and Choi model [29] was adopted in the present study and implemented in ANSYS Fluent through a UDF to ensure consistency with the established nanofluid literature [33–35]. Unlike assigning a constant thermal conductivity, the UDF evaluates the effective thermal conductivity locally within every computational cell using the local nanoparticle volume fraction. Accordingly, the thermal conductivity is continuously updated during the iterative solution process, allowing the CFD solver to account for the spatial variation of the nanofluid thermophysical properties throughout the computational domain. The transport equation for nanoparticle volume fraction is given by:

$$\nabla \cdot (\alpha_p \rho_p \vec{V}_m) = -\nabla \cdot (\alpha_p \rho_p \vec{V}_{dr,p}) \quad (15)$$

where α_p is the nanoparticle volume fraction, ρ_p is the nanoparticle density, $\vec{V}_m$ is the mixture velocity, and $\vec{V}_{dr,p}$ is the nanoparticle drift velocity relative to the mixture. The mixture model allows prediction of local nanoparticle concentration distributions and provides a more physically representative description of nanoparticle transport behavior compared to the homogeneous single-phase approach.

2.4. Investigated Cases

The thermophysical properties of the nanoparticles employed in the present study are summarized in Table 1, whereas the thermophysical properties of the base fluid (Therminol LT heat transfer oil) are listed in Table 2. Following validation, both SP and TP formulations were retained for the comparative parametric investigation. Three nanoparticle materials, namely Cu, CuO, and TiO_2, were subsequently investigated at five nanoparticle volume fractions of 1%, 2%, 3%, 5%, and 6%, resulting in a total of 15 simulation cases. The objective of this investigation was to evaluate the influence of nanoparticle type and concentration on the thermal and hydraulic performance of the shell-and-tube heat exchanger under identical operating condition. Cu, CuO, and TiO_2 nanoparticles were selected because they represent three widely used nanomaterials with distinct thermophysical characteristics, including high thermal conductivity (Cu), balanced thermal performance and cost (CuO), and excellent chemical stability (TiO_2) [36,37].

Table 1: Thermophysical characteristics of some nanoparticles [29,30].

Material	Thermal conductivity (k) (W/m.K)	Density (ρ) (kg/m^3)	Specific heat capacity (C_p) (J/kg. K)
Copper	393	8934	397
Copper-oxide	33	6000	550
Titanium-dioxide	8.4	4230	690

Table 2: Thermophysical characteristics of base fluid [27].

Material	Thermal conductivity (k) (W/m.K)	Density (ρ) (kg/m^3)	Specific heat capacity (C_p) (J/kg. K)	Dynamic viscosity (μ) (kg/m.s)
Therminol oil	0.0999	759.5	2250	2.73×10^{-4}

2.5. Performance Evaluation Parameters

The thermal and hydraulic performance of the investigated nanofluids was evaluated using the Reynolds number, Peclet number, heat transfer rate, overall heat transfer coefficient, pressure drop, and the Performance Evaluation Criterion (PEC). The Reynolds number was calculated as $Re = \rho * v * d/\mu$ while the Peclet number was determined as $Pe = Re * Pr$ [38]. The heat transfer rate was obtained from the energy balance, $\dot{Q} = \dot{m} * Cp * \Delta T$, and the overall heat transfer coefficient was subsequently calculated using the logarithmic mean temperature difference (LMTD) method as $U = Q/A\Delta T_{lmtd}$ [1]. The combined thermal–hydraulic performance was then evaluated using the Performance Evaluation Criterion (PEC) [39,40]:

$$PEC = \frac{\frac{U_{nf}}{U_f}}{(\frac{f_{nf}}{f_f})^{\frac{1}{3}}} \tag{16}$$

where PEC is the performance evaluation criterion, U_{nf} and U_f are the overall heat transfer coefficients of the nanofluid and basal fluid, respectively. f_{nf} and f_f represent the friction factors of the nanofluid and basal fluid, respectively.

2.6. Boundary Conditions

Uniform velocity-inlet boundary conditions were specified at both fluid inlets. The hot oil-based nanofluid entered the tube side with a uniform inlet velocity of 1.5 m/s and a constant temperature of 418 K, whereas cold water entered the shell side in a counter-flow arrangement with a uniform inlet velocity of 0.3 m/s and a constant temperature of 333 K. Pressure-outlet boundary conditions with zero gauge pressure were imposed at both the tube-side and shell-side outlets. The inlet turbulence intensity was specified as 5%, which is adopted for turbulent internal flows and has been employed in previous CFD investigations of shell-and-tube heat exchangers [41,42]. To evaluate the influence of the assumed inlet turbulence level, additional simulations were performed using turbulence intensities of 2%, 5%, and 10%. The predicted thermal and hydraulic results exhibited negligible differences. All solid walls were treated as stationary no-slip boundaries. The external shell wall was assumed to be adiabatic. For the two-phase simulations, the base oil was defined as the primary phase and the nanoparticles as the dispersed secondary phase. The nanoparticle volume fraction was specified uniformly at the tube-side inlet according to the investigated concentration (1–6 vol.%), whereas no nanoparticles were introduced through the shell-side inlet.

2.7. Turbulence Model

The flow inside the shell-and-tube heat exchanger remained turbulent under all investigated operating conditions, with the Reynolds number varying from approximately 13,000 to 19,000. Accordingly, the realizable k–ε turbulence model was employed to simulate the turbulent flow and heat transfer characteristics. The realizable k–ε model was selected because it provides improved accuracy for complex internal flows involving separation, recirculation, rotation, and adverse pressure gradients, which are characteristic of the shell-side flow through segmental baffles. In addition, the model has been extensively validated and widely adopted in numerical investigations of shell-and-tube heat exchangers owing to its favorable balance between computational efficiency and predictive accuracy [41,42]. Several turbulence models, including the Standard k–ε, RNG k–ε, Realizable k–ε, and Reynolds Stress Model (RSM), were preliminarily evaluated under identical operating conditions. Since all investigated models produced nearly identical thermal predictions, the realizable k–ε model was selected because it provided the best compromise between prediction accuracy, numerical stability, and computational efficiency.

2.8. Grid Independence

A grid independence study was performed to ensure that the numerical results were independent of the computational mesh. Five computational meshes with progressively increasing numbers of cells were generated and evaluated under identical operating conditions. The cold-water outlet temperature was selected as the monitoring parameter because it directly reflects the overall heat transfer performance of the heat exchanger. The comparison was carried out using pure Therminol LT as the hot working fluid without nanoparticle addition in order to eliminate the influence of varying thermophysical properties. The predicted cold-water outlet temperature became nearly unchanged with further mesh refinement beyond approximately 2.8 million cells, indicating that the numerical solution was independent of the mesh. Therefore, the mesh containing approximately 2.8 million cells was adopted for all subsequent simulations as it provided a suitable compromise between computational accuracy and computational cost. The variation of the predicted cold-water outlet temperature with the total number of computational cells is presented in Figure 2.

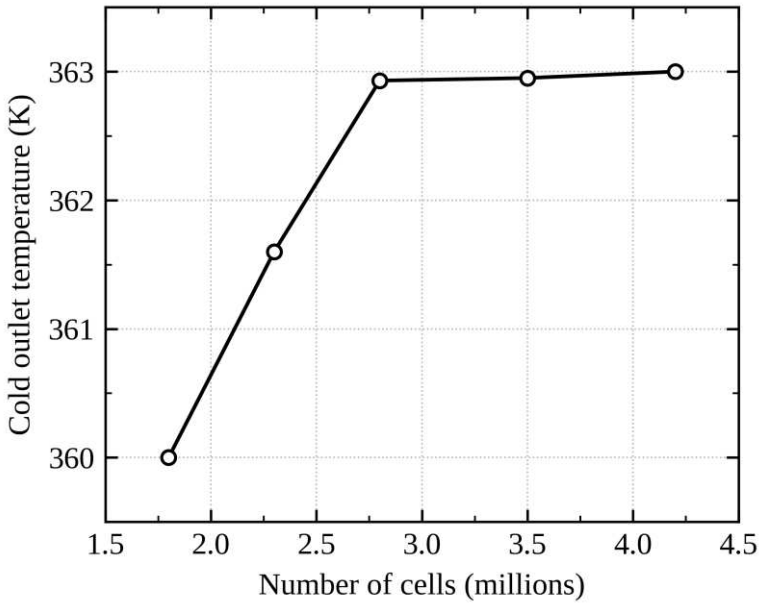


Figure 2: Outlet temperature of the cold fluid at different number of cells.

3. Validation of Numerical Methodology

3.1. Experimental Benchmark Description

The numerical methodology was validated against the experimental measurements reported by Farajollahi et al. [24], who investigated turbulent heat transfer of Al_2O_3/water nanofluids in a shell-and-tube heat exchanger with geometry and operating conditions comparable to those considered in the present study. The benchmark was selected because it provides experimentally measured overall heat transfer coefficients over a wide range of Reynolds and Peclet numbers, making it suitable for assessing the accuracy of the developed CFD model. Al_2O_3 nanoparticles with a particle diameter of 25 nm were dispersed in water at volume concentrations of 0.3%, 0.5% and 2%.

The validation was performed by comparing the predicted overall heat transfer coefficients obtained from both the single-phase (SP) and two-phase (TP) formulations with the corresponding experimental measurements. In addition, analytical predictions based on conventional turbulent heat transfer correlations $Nu = 0.012(Re^{0.87} - 280)Pr^{0.4}$ were included to provide an independent reference for evaluating the physical consistency of both CFD formulations.

Figure 3, Figure 4, and Figure 5 compare the SP and TP predictions with the experimental measurements of Farajollahi et al [24]. and the corresponding analytical solution. Both formulations successfully reproduced the experimental trend over the investigated Peclet-number range. However, the TP formulation consistently provided closer agreement with the experimental data, with MAPE values of 7.14%, 9.23%, and 15.02% at nanoparticle volume fractions of 0.3%, 0.5%, and 2%, respectively, compared with 9.37%, 9.38%, and 16.47% for the SP formulation. The prediction error increased with increasing nanoparticle concentration for both formulations, which is consistent with previous studies reporting that

higher nanoparticle concentrations intensify particle interactions and increase the complexity of nanoparticle transport, leading to larger deviations between numerical predictions and experimental measurements [43,44]. Furthermore, the deviation between the numerical and experimental results decreased with increasing Peclet number. This trend has also been reported in the literature and is attributed to the increasing dominance of turbulent convective transport over nanoparticle diffusion, resulting in stronger particle–fluid coupling and enhanced mixing at higher Peclet numbers. Conversely, larger deviations at lower Peclet numbers are commonly associated with entrance-region effects and the greater influence of local transport phenomena in the developing flow region [45,46].

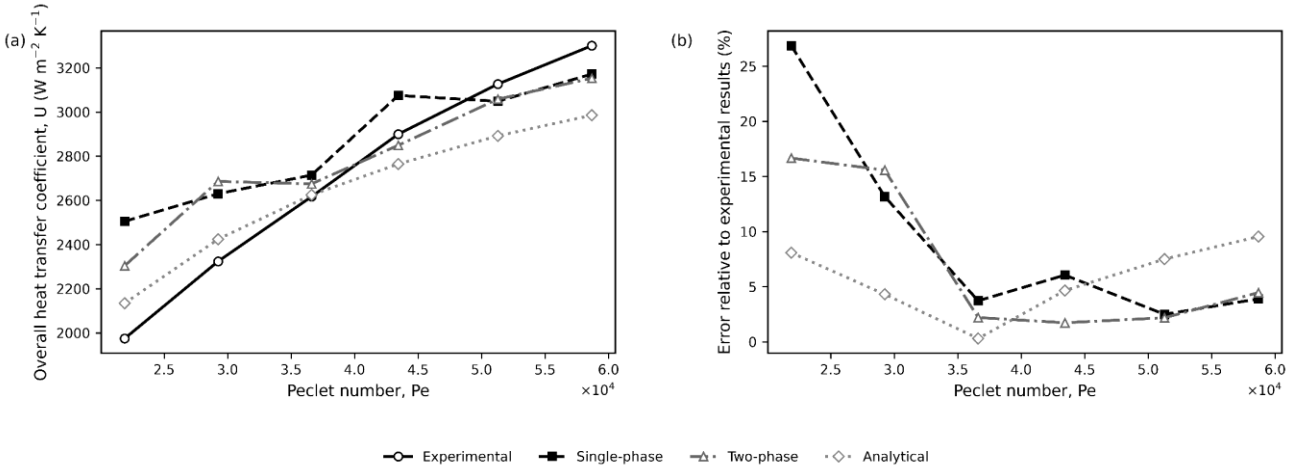


Figure 3: Validation results for the different simulation and analytical results for Al_2O_3 nanoparticles' volume concentration of 0.3%: (a) Overall heat transfer coefficient, (b) Error percentage with respect to experimental results.

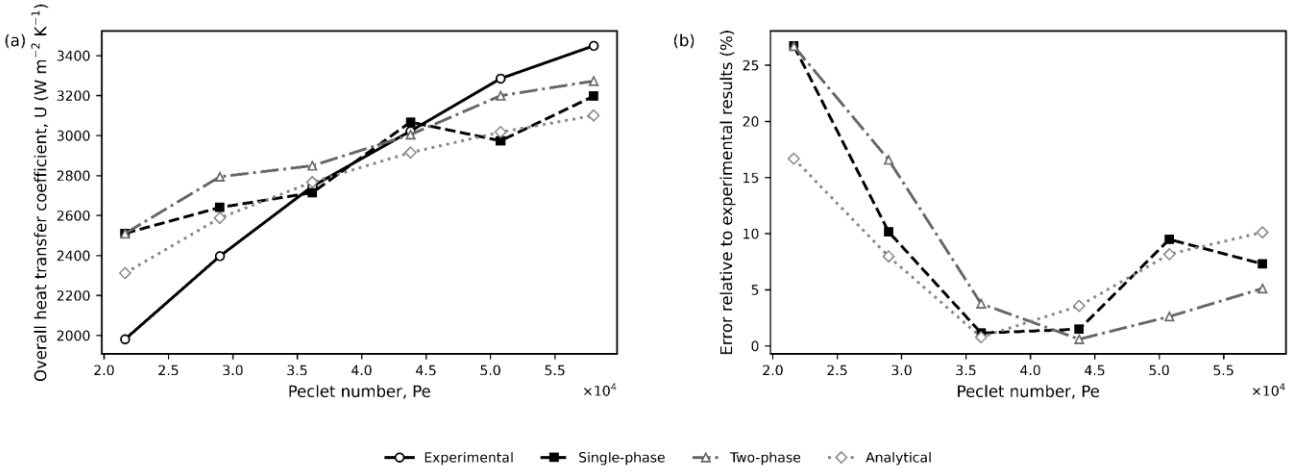


Figure 4: Validation results for the different simulation and analytical results for Al_2O_3 nanoparticles' volume concentration of 0.5%: (a) Overall heat transfer coefficient, (b) Error percentage with respect to experimental results.

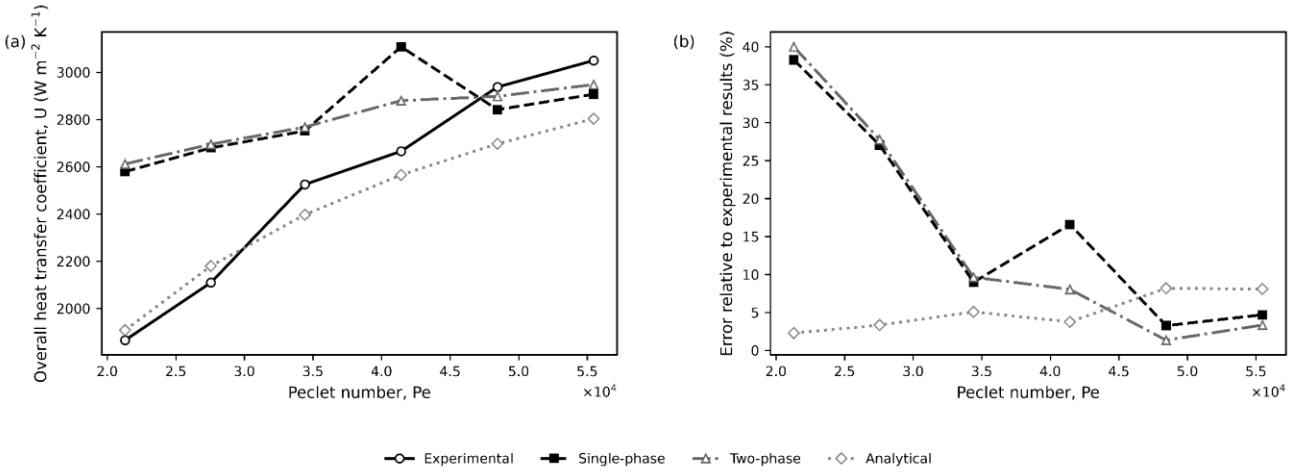


Figure 5: Validation results for the different simulation and analytical results for Al_2O_3 nanoparticles' volume concentration of 2%: (a) Overall heat transfer coefficient, (b) Error percentage with respect to experimental results.

4. Results and Discussion

4.1. Thermal Performance

The thermal performance predicted by the single-phase (SP) and two-phase (TP) formulations for Cu, CuO, and TiO_2 oil-based nanofluids is presented in Figure 6 in terms of the overall heat transfer coefficient. This parameter provides complementary indicator of the heat transfer enhancement achieved through nanoparticle addition. For all investigated nanofluids, increasing the nanoparticle concentration initially enhanced the overall heat transfer coefficient. This behavior is primarily attributed to the increase in the effective thermal conductivity of the nanofluid, which improves heat transfer between the hot oil flowing inside the tubes and the cold water circulating through the shell side. A consistent difference was observed between the SP and TP predictions, with the SP formulation predicting higher overall heat transfer coefficients than the TP formulation for all investigated nanoparticle types and concentrations. This behavior can be attributed to the homogeneous effective-property assumption employed in the SP model, where the nanofluid is treated as a single continuum phase with enhanced thermophysical properties. Consequently, the thermal enhancement associated with nanoparticle addition is directly incorporated into the governing equations, leading to higher predicted heat transfer rates [15]. In contrast, the TP formulation accounts for nanoparticle transport and phase-distribution effects, resulting in lower thermal predictions that agreed more closely with the selected experimental benchmark. Compared with the pure oil case, the addition of nanoparticles resulted in a measurable enhancement in the overall heat transfer coefficient for both formulations. For the SP model, the maximum enhancement reached approximately 10.7%, 4.9%, and 3.9% for Cu, CuO, and TiO_2 nanofluids, respectively. The corresponding maximum enhancements predicted by the TP formulation were approximately 3.8%, 2.8%, and 2.5%. These results further demonstrate the tendency of the SP model to predict greater thermal enhancement than the TP formulation. Among the investigated nanofluids, Cu

exhibited the highest overall heat transfer coefficients, followed by CuO and TiO_2. This ranking was consistently observed for both SP and TP formulations and reflects the superior thermal conductivity of Cu nanoparticles compared with CuO and TiO_2. The highest overall heat transfer coefficient predicted by the SP formulation was approximately 1803 W/m² ·K for Cu nanofluids at a concentration of 5 vol.%, whereas the maximum value predicted by the TP formulation was approximately 1692 W/m² ·K for Cu nanofluids at a concentration of 3 vol.%. The cold-fluid outlet temperature followed the same trend as the overall heat transfer coefficient. In all cases, the SP formulation predicted slightly higher outlet temperatures than the TP formulation, and Cu nanofluids produced the highest values, followed by CuO and TiO_2. For both formulations, thermal performance improved with increasing nanoparticle concentration up to an optimum value and then decreased after 5 vol.% for SP and 3 vol.% for TP, indicating that the beneficial effect of thermal conductivity enhancement was progressively offset at high concentrations by the accompanying increase in viscosity [24,44]. Accordingly, the predicted optimum concentration depended on the selected CFD formulation.

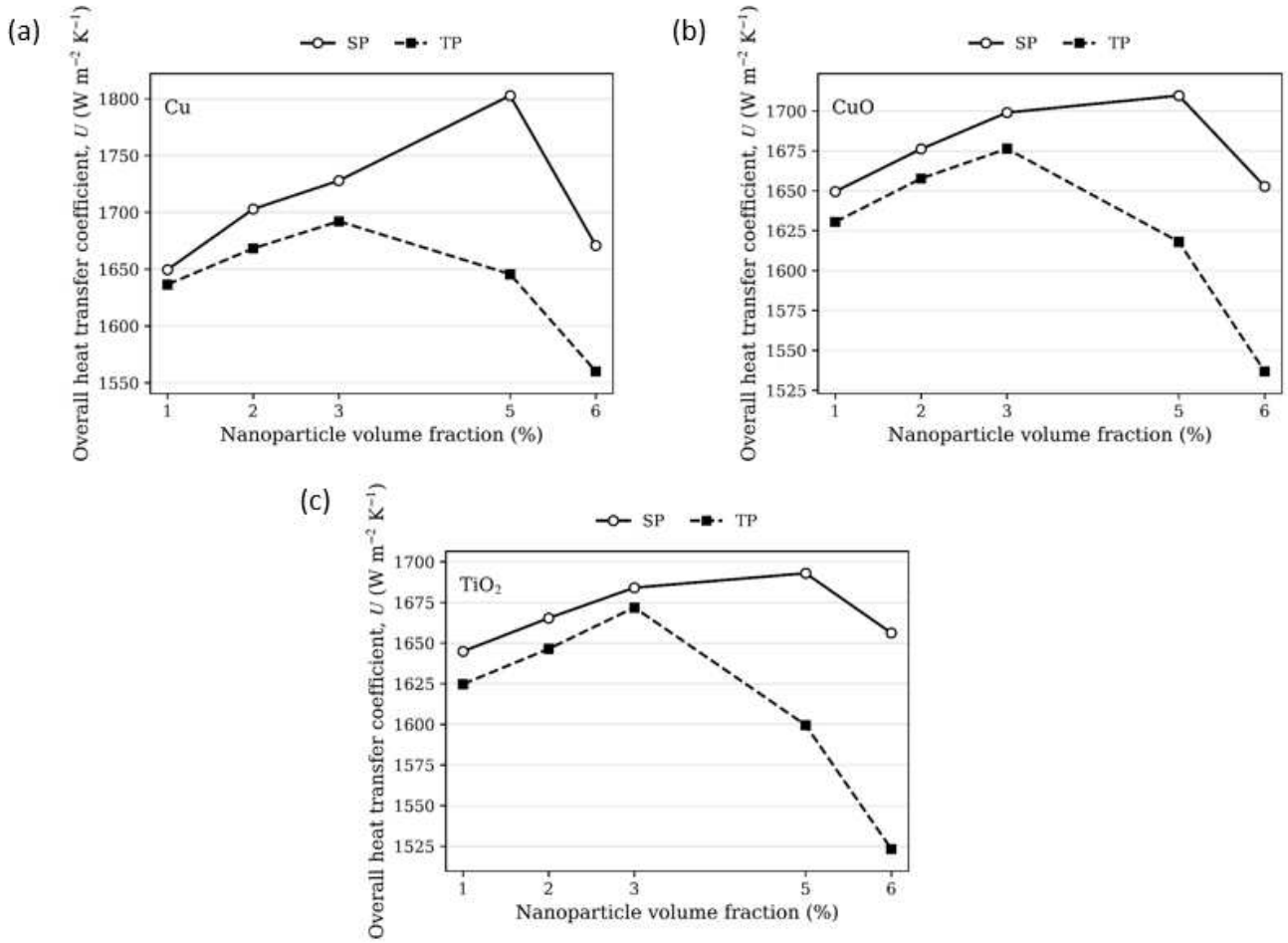


Figure 6: Variation of the overall heat transfer coefficient with nanoparticle volume fraction for (a) Cu, (b) CuO, and (c) TiO_2 nanofluids.

4.2. Pressure Drop Characteristics

Figure 7 compares the variation of tube-side pressure drop with nanoparticle concentration for Cu, CuO, and TiO_2 nanofluids using both the single-phase (SP) and two-phase (TP) formulations. For all investigated nanofluids, the pressure drop increased continuously with increasing nanoparticle concentration. Compared with the pure oil case, nanoparticle addition resulted in a noticeable increase in flow resistance due to the corresponding increase in nanofluid viscosity. As the nanoparticle concentration increased, higher frictional losses developed inside the tubes, leading to larger pressure drops and consequently higher pumping power requirements. Among the investigated nanofluids, Cu produced the highest pressure-drop values, followed by CuO and TiO_2. For the SP formulation, the pressure drop increased from approximately 23.0 kPa for pure oil to approximately 38.4 kPa for Cu nanofluids at 6 vol.%, corresponding to an increase of approximately 67%. Similar trends were observed for the TP formulation. This is because Cu nanoparticles alter the nanofluid's effective viscosity and density more strongly than CuO or TiO_2, increasing flow resistance, highlighting the trade-off between enhanced heat transfer and higher pumping power requirements. A comparison between the SP and TP formulations revealed extremely small differences in pressure-drop predictions throughout the investigated concentration range. For example, the pressure drop predicted for Cu nanofluids at 6 vol.% was approximately 38.36 kPa and 38.34 kPa for the SP and TP formulations, respectively. Similar agreement was observed for CuO and TiO_2 nanofluids. These results indicate that the hydraulic behavior of the investigated nanofluids is largely insensitive to the selected CFD formulation. This observation contrasts with the thermal performance results discussed in Section 4.1, where noticeable differences were observed between the SP and TP predictions of the overall heat transfer coefficient and cold-fluid outlet temperature. While the SP formulation consistently predicted higher thermal enhancement than the TP formulation, both formulations produced nearly identical pressure-drop values. The divergence between the SP and TP formulations in thermal performance, in contrast to their close agreement in pressure drop, can be attributed to the different physical mechanisms governing each quantity. Pressure drop is primarily controlled by the bulk momentum balance, which depends on the mixture-averaged density and viscosity; since both formulations predict nearly identical bulk mixture rheology, they yield comparable friction factors and pressure drops. Heat transfer, however, is governed by the thermal boundary layer near the wall, where local nanoparticle concentration gradients play a decisive role. The TP formulation resolves these mechanisms explicitly, allowing local variations in nanoparticle concentration near the wall that alter the near-wall thermal conductivity and viscosity gradients. Since these effects have only a secondary influence on the bulk momentum balance but a first-order influence on the thermal boundary layer, the two formulations converge for pressure drop while diverging for thermal performance. Therefore, the influence of CFD formulation appears to be considerably more significant for thermal transport prediction than for hydraulic performance prediction. It is also evident that the increase in pressure drop continued throughout the investigated concentration range, even in cases where the thermal performance began to deteriorate at higher concentrations. Consequently, increasing nanoparticle concentration beyond the optimum value results in a larger hydraulic penalty

without a corresponding thermal benefit. This behavior explains the reduction in thermal–hydraulic performance observed at high concentrations and highlights the importance of balancing heat transfer enhancement against pumping power requirements when selecting the optimum nanoparticle concentration.

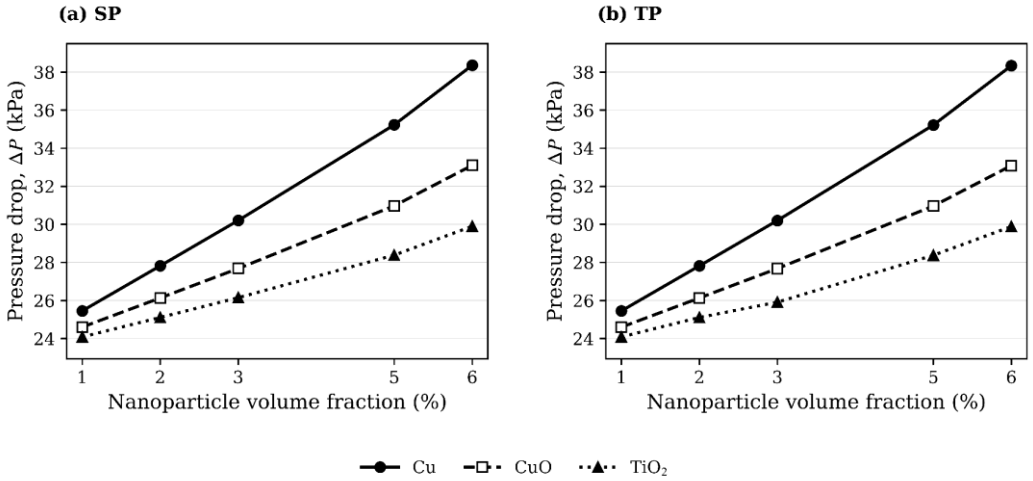


Figure 7: Variation of tube-side pressure drop with nanoparticle volume fraction for Cu, CuO, and TiO_2 nanofluids predicted using (a) SP and (b) TP formulations.

4.3. Thermal-Hydraulic Performance

To evaluate the combined thermal and hydraulic performance of the investigated nanofluids, the Performance Evaluation Criterion (PEC) was calculated based on the overall heat transfer coefficient according to Eq. (16). The PEC provides a comprehensive assessment of thermal enhancement relative to the corresponding hydraulic penalty and therefore represents a practical indicator for heat exchanger performance optimization. Figure 8 compares the variation of PEC with nanoparticle concentration for Cu, CuO, and TiO_2 nanofluids using both the single-phase (SP) and two-phase (TP) formulations. For all investigated nanofluids, the PEC initially increased with increasing nanoparticle concentration, indicating that the thermal enhancement obtained from nanoparticle addition exceeded the associated increase in flow resistance. This behavior confirms that, at low and moderate concentrations, the improvement in heat transfer performance is greater than the corresponding hydraulic penalty. Among the investigated nanofluids, Cu consistently exhibited the highest PEC values, followed by CuO and TiO_2. This ranking was observed for both SP and TP formulations and is consistent with the superior thermal performance of Cu nanoparticles discussed in Section 4.1. The maximum PEC values predicted by the SP formulation were approximately 1.108, 1.049, and 1.038 for Cu, CuO, and TiO_2 nanofluids, respectively. The corresponding maximum PEC values predicted by the TP formulation were approximately 1.040, 1.029, and 1.028. These results indicate that Cu nanoparticles provide the most favorable balance between heat transfer enhancement and hydraulic penalty under the investigated operating conditions. Although the nanoparticle ranking remained unchanged, noticeable differences were observed in the predicted optimum concentration. The SP formulation predicted maximum thermal–hydraulic performance at approximately 5 vol.%

for all investigated nanofluids, whereas the TP formulation predicted optimum performance at approximately 3 vol.%. This discrepancy can be attributed to the tendency of the SP model to predict higher thermal enhancement than the TP formulation, particularly at higher concentrations. Beyond the optimum concentration, the PEC decreased for all investigated nanofluids with the continued increase in pressure drop. This behavior can be explained by the combined trends observed in Sections 4.1 and 4.2. At high nanoparticle concentrations, the increase in viscosity causes a substantial increase in hydraulic losses, while the deterioration of U-values becomes progressively more pronounced. Overall, the results indicate that both SP and TP formulations identify the same optimum nanoparticle type, namely Cu. However, the selected CFD formulation significantly influences the predicted optimum concentration and the magnitude of thermal–hydraulic enhancement. Therefore, the choice of CFD formulation may affect optimization studies and engineering decisions involving nanofluid-based shell-and-tube heat exchangers.

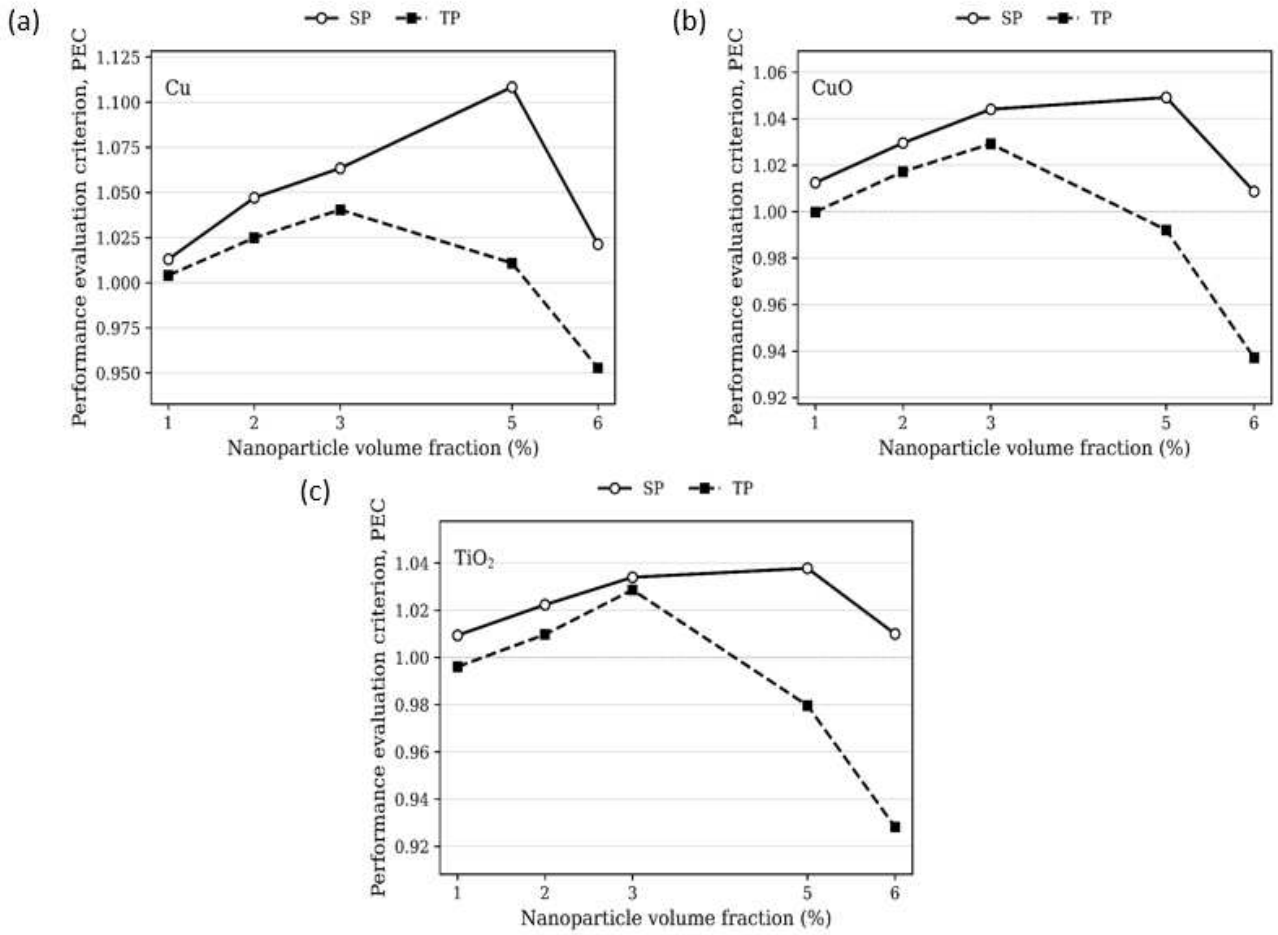


Figure 8: Variation of the performance evaluation criterion with nanoparticle volume fraction for (a) Cu, (b) CuO, and (c) TiO_2 nanofluids.

4.4. Nanoparticles-Fluid Slip Velocity Analysis

The relative motion between the nanoparticles and the base fluid was evaluated using the slip-velocity magnitude:

$$\nabla V_{slip} = |V_p - V_f| \quad (17)$$

where V_p and V_f denote the nanoparticle- and fluid-phase velocity vectors, respectively. The maximum particle–fluid slip velocity ranged from 7.63×10^{-7} to 1.94×10^{-6} m. s^{-1}. Relative to the tube-side inlet velocity of 1.5 m. s^{-1}, the maximum slip ratio was approximately 1.29×10^{-4}%, confirming strong kinematic coupling between the phases. This behavior is expected for nanoscale particles because their small inertia and short response time allow the interphase drag force to rapidly adjust their velocity to that of the surrounding liquid.

The negligible slip velocity indicates that relative particle–fluid motion has little influence on the bulk momentum balance. This finding is consistent with the nearly identical pressure drops predicted by the SP and TP formulations in the present study. Similar behavior was reported by Akbari et al. [15], who found that single- and two-phase nanofluid models could predict almost identical hydrodynamic fields while producing appreciably different thermal predictions. Buongiorno [43] also demonstrated that conventional inertial, gravitational, and other mechanical slip mechanisms are generally weak for nanoscale suspensions.

Although particle–fluid slip and nanoparticle redistribution were negligible, differences remained between the SP and TP thermal predictions because the two formulations treated the phase properties and energy transport differently. In the SP formulation, the nanofluid was represented as a homogeneous continuum with effective properties evaluated at the prescribed bulk concentration and applied uniformly throughout the tube-side domain. In contrast, the TP mixture formulation retained the nanoparticle phase through its volume-fraction transport equation and phase-weighted mixture equations, while the effective properties were evaluated locally through UDFs. This formulation-dependent property and energy coupling produced differences in the predicted temperature field and wall heat flux, even though the phases moved at almost identical velocities. Conversely, the bulk velocity and effective viscosity fields remained similar, leading to nearly identical pressure-drop predictions [47]. Consequently, differences in the calculated overall heat transfer coefficient may arise even when the two phases move at almost the same velocity [10]. The present slip-velocity results therefore indicate that the thermal differences between SP and TP should primarily be associated with their different thermophysical-property and energy-transfer formulations rather than substantial particle–fluid velocity slip.

4.5. Engineering Implications of Single-Phase and Two-Phase Modeling

The results indicate that the selected formulation affects thermal predictions more strongly than hydraulic predictions. The SP formulation predicts higher overall heat transfer coefficients than the TP formulation, whereas both approaches yield nearly identical pressure drops because the phases remain strongly coupled and the nanoparticle distribution is essentially uniform. Both formulations identify Cu as the best-performing nanoparticle, but

they predict different optimum concentrations. From an engineering perspective, SP simulations remain suitable for preliminary screening and rapid parametric studies because of their simpler implementation. Under the investigated conditions, the TP formulation provided closer agreement with the experimental benchmark and may therefore be preferred when more detailed thermal prediction and nanoparticle-concentration optimization are required. Nevertheless, the comparison should be interpreted as reflecting both the phase formulation and the associated local-property implementation.

5. Conclusions

A comparative CFD investigation of single-phase (SP) and two-phase (TP) formulations was conducted for Cu-, CuO-, and TiO_2–Therminol LT nanofluids flowing through a shell-and-tube heat exchanger. The numerical methodology was assessed against published experimental measurements and analytical heat-transfer calculations. The TP formulation produced lower errors relative to the selected experimental benchmark, while both formulations reproduced the experimental trends and agreed reasonably with the analytical predictions. The SP formulation consistently predicted higher overall heat transfer coefficients, heat-transfer rates, and cold-fluid outlet temperatures than the TP formulation. For Cu nanofluids, the maximum enhancement in the overall heat transfer coefficient relative to pure oil was approximately 10.7% using SP and 3.8% using TP. The predicted particle–fluid slip velocities were only of the order of 10^{-7}–10^{-6} ms^{-1}, while the nanoparticle volume fraction remained essentially uniform throughout the tube-side fluid region. Therefore, the thermal differences between the formulations cannot be attributed primarily to substantial particle migration or velocity slip. Instead, they reflect the different numerical treatment of the phases and thermophysical properties: the SP formulation applies effective properties uniformly at the prescribed bulk concentration, whereas the TP mixture formulation retains secondary-phase transport and evaluates the effective properties locally within the mixture equations. In contrast, SP and TP produced nearly identical pressure-drop predictions because the phases remained strongly coupled and their bulk velocity and effective-viscosity fields were similar. The PEC assessment identified Cu as the most favorable nanoparticle, followed by CuO and TiO_2, under both formulations. However, the optimum concentration differed, with SP predicting maximum thermal–hydraulic performance at approximately 5 vol.% and TP at approximately 3 vol.%. Beyond these concentrations, PEC decreased because the continued increase in viscosity and hydraulic losses outweighed the additional thermal benefit.

Key findings:

- The TP formulation produced lower MAPE values than SP relative to the selected experimental benchmark, while both formulations reproduced the experimental trends and agreed reasonably with the analytical calculations.
- SP predicted greater thermal enhancement than TP for all investigated nanoparticle types and concentrations; the maximum overall heat transfer coefficient enhancement for Cu was approximately 10.7% using SP and 3.8% using TP.

- Particle–fluid slip velocities were of the order of 10^{-7}–10^{-6} m s^{-1}, and the nanoparticle distribution remained essentially uniform, indicating strong phase coupling and negligible nanoparticle redistribution.
- The thermal differences between SP and TP were therefore associated primarily with their different phase representation and local thermophysical-property treatment rather than substantial particle migration.
- Cu provided the greatest thermal and thermal–hydraulic performance, followed by CuO and TiO_2, and this ranking was unchanged by the selected CFD formulation.
- Pressure drop increased continuously with nanoparticle concentration but remained nearly identical between SP and TP, demonstrating that hydraulic prediction was substantially less sensitive to the CFD formulation than thermal prediction.
- SP and TP predicted different optimum concentrations—approximately 5 vol.% and 3 vol.%, respectively—showing that the modeling approach can influence thermal–hydraulic optimization outcomes.
- The decline in PEC beyond the optimum concentration confirms that increasing nanoparticle loading does not necessarily improve overall performance because the growing hydraulic penalty eventually outweighs the thermal benefit.

Overall, SP is suitable for preliminary screening and rapid parametric assessment because of its simpler implementation, whereas TP may be preferred when a more detailed representation of the dispersed phase and locally evaluated properties is required. This recommendation is limited to the models, property correlations, and operating conditions investigated in the present study.

Future investigations may include transient nanofluid simulations to capture time-dependent thermal–hydraulic behavior, the implementation of advanced multiphase formulations — such as full Eulerian–Eulerian two-fluid models with explicit inter-phase momentum and energy exchange, Lagrangian discrete-phase tracking, or population balance modeling to more accurately capture nanoparticle migration, agglomeration, and localized concentration effects that influence thermal–hydraulic performance, experimental validation under different operating conditions to further verify the predictive capability of the numerical models, and investigation of non-Newtonian nanofluid behavior in shell-and-tube heat exchangers.

Statements & Declarations

Funding

The authors declare that no funds, grants, or other support were received during the preparation of this manuscript.

Competing Interests

The authors have no relevant financial or non-financial interests to disclose.

References

[1] Dewitt LI. Fundamentals of Heat and Mass Transfer. 06 ed. NewYork: John Wiley & Sons; 2007.

[2] H. Banka, V. Reddy MR. CFD Analysis of Shell and Tube Heat Exchanger using Titanium Carbide, Titanium Nitride and Zinc Oxide Nanofluids. Int J Innov Eng Technol 2016:315–22. https://doi.org/10.12735/ijiet.v6i11.304.

[3] Jeevanandam J, Barhoum A, Chan YS, Dufresne A, Danquah MK. Review on nanoparticles and nanostructured materials: History, sources, toxicity and regulations. Beilstein J Nanotechnol 2018;9:1050–74. https://doi.org/10.3762/bjnano.9.98.

[4] Firlianda DA, Permanasari AA, Puspitasari P, Sukarni S. Heat transfer enhancement using nanofluids (MnFe2O4-ethylene glycol) in mini heat exchanger shell and tube. AIP Conf Proc 2019;2120. https://doi.org/10.1063/1.5115690.

[5] Eastman JA, Choi SUS, Li S, Yu W, Thompson LJ. Anomalously increased effective thermal conductivities of ethylene glycol-based nanofluids containing copper nanoparticles. Appl Phys Lett 2001;78:718–20. https://doi.org/10.1063/1.1341218.

[6] M.M. Alqarni, Muhammaad Ibrahim, Taghreed A. Assiri, Tareq Saeed, Abd Allah A. Mousa VA. Two-phase simulation of a shell and tube heat exchanger filled with hybrid nanofluid. Eng Anal Bound Elem 2023;146:80–8. https://doi.org/10.1016/j.enganabound.2022.10.001.

[7] Nagarajan PK, Subramani J, Suyambazhahan S, Sathyamurthy R. Nanofluids for solar collector applications: A review. Energy Procedia 2014;61:2416–34. https://doi.org/10.1016/j.egypro.2014.12.017.

[8] Sharafeldin MA, Gróf G, Abu-Nada E, Mahian O. Evacuated tube solar collector performance using copper nanofluid: Energy and environmental analysis. Appl Therm Eng 2019;162:114205. https://doi.org/10.1016/j.applthermaleng.2019.114205.

[9] Li Y. Molecular design of photovoltaic materials for polymer solar cells: Toward suitable electronic energy levels and broad absorption. Acc Chem Res 2012;45:723–33. https://doi.org/10.1021/ar2002446.

[10] Liang G, Mudawar I. Review of single-phase and two-phase nanofluid heat transfer in macro-channels and micro-channels. Int J Heat Mass Transf 2019;136:324–54. https://doi.org/10.1016/j.ijheatmasstransfer.2019.02.086.

[11] Abed N, Afgan I, Nasser A, Iacovides H, Cioncolini A, Mekhail T. Numerical Investigations of parabolic trough collectors using different nanofluids. Int J Appl Energy Syst 2020;2:88–94. https://doi.org/10.21608/ijaes.2020.169898.

[12] Peyghambarzadeh SM, Hashemabadi SH, Jamnani MS, Hoseini SM. Improving the cooling performance of automobile radiator with Al 2O3/water nanofluid. Appl Therm Eng 2011;31:1833–8. https://doi.org/10.1016/j.applthermaleng.2011.02.029.

[13] Hussein AM, Sharma K V., Bakar RA, Kadirgama K. A review of forced convection heat transfer enhancement and hydrodynamic characteristics of a nanofluid. Renew

Sustain Energy Rev 2014;29:734–43. https://doi.org/10.1016/j.rser.2013.08.014.

[14] Behzadmehr A, Saffar-Avval M, Galanis N. Prediction of turbulent forced convection of a nanofluid in a tube with uniform heat flux using a two phase approach. Int J Heat Fluid Flow 2007;28:211–9. https://doi.org/10.1016/j.ijheatfluidflow.2006.04.006.

[15] Akbari M, Galanis N, Behzadmehr A. Comparative analysis of single and two-phase models for CFD studies of nanofluid heat transfer. Int J Therm Sci 2011;50:1343–54. https://doi.org/10.1016/j.ijthermalsci.2011.03.008.

[16] Hamed Eshgarf, Afshin Ahmadi Nadooshan AR. A review of multi-phase and single-phase models in the numerical simulation of nanofluid flow in heat exchangers. Eng Anal Bound Elem 2023;146:910–27. https://doi.org/10.1016/j.enganabound.2022.10.013.

[17] Yousef Abdollahzadeh, Mehdi Mehrpooya, Seyed Mohammad Ali Mousavian HM. Modeling and simulation of nanofluid in low Reynolds numbers using two-phase Lattice Boltzmann method based on mixture model. Chem Eng Res Des 2023;192:402–11. https://doi.org/10.1016/j.cherd.2023.02.023.

[18] Sanei F, M. Ali AB, Jasim DJ, Salahshour S, Akbari OA, Emami N. Numerical simulation of the nanofluid flow and heat transfer in porous microchannels with different flow path arrangements using single-phase and two-phase models. Int J Thermofluids 2024;24:100846. https://doi.org/10.1016/j.ijft.2024.100846.

[19] Lotfi R, Saboohi Y, Rashidi AM. Numerical study of forced convective heat transfer of Nanofluids: Comparison of different approaches. Int Commun Heat Mass Transf 2010;37:74–8. https://doi.org/10.1016/j.icheatmasstransfer.2009.07.013.

[20] Ying Z, He B, He D, Kuang Y, Ren J, Song B. Comparisons of single-phase and two-phase models for numerical predictions of Al2O3/water nanofluids convective heat transfer. Adv Powder Technol 2020;31:3050–61. https://doi.org/10.1016/j.apt.2020.05.032.

[21] Bianco V, Manca O, Nardini S. Numerical investigation on nanofluids turbulent convection heat transfer inside a circular tube. Int J Therm Sci 2011;50:341–9. https://doi.org/10.1016/j.ijthermalsci.2010.03.008.

[22] Mezrakchi R Al. Investigation of various hybrid nanofluids to enhance the performance of a shell and tube heat exchanger. AIMS Energy 2024;12:235–55. https://doi.org/10.3934/energy.2024011.

[23] Marzouk SA, Abou Al-Sood MM, El-Said EMS, Younes MM, El-Fakharany MK. A comprehensive review of methods of heat transfer enhancement in shell and tube heat exchangers. J Therm Anal Calorim 2023;148:7539–78. https://doi.org/10.1007/s10973-023-12265-3.

[24] Farajollahi B, Etemad SG, Hojjat M. Heat transfer of nanofluids in a shell and tube heat exchanger. Int J Heat Mass Transf 2010;53:12–7. https://doi.org/10.1016/j.ijheatmasstransfer.2009.10.019.

[25] Gnielinski V. New equations for heat and mass transfer in turbulent pipe and channel flow. Int Chem Eng 1976;16:359–68.

[26] Klazly M, Mahabaleshwar US, Bognár G. Comparison of single-phase Newtonian and non-Newtonian nanofluid and two-phase models for convective heat transfer of nanofluid flow in backward-facing step. J Mol Liq 2022;361:119607. https://doi.org/10.1016/j.molliq.2022.119607.

[27] Ozgen F, Kamaci G. Numerical heat transfer from Al2O3/water nanofluid through square cross-sectional duct with single- and two-phase models. J Therm Anal Calorim 2022;147:13483–98. https://doi.org/10.1007/s10973-022-11539-6.

[28] Hassaan AM. Evaluating experimentally the viability of employing hybrid nanofluids as an operating fluid in a shell-and-tube heat exchanger. Sci Rep 2025;15. https://doi.org/10.1038/s41598-025-87149-7.

[29] Yu W, Choi SUS. The role of interfacial layers in the enhanced thermal conductivity of nanofluids: A renovated Maxwell model. J Nanoparticle Res 2003;5:167–71. https://doi.org/10.1023/A:1024438603801.

[30] Xie H, Wang J, Xi T, Liu Y, Ai F, Wu Q. Thermal conductivity enhancement of suspensions containing nanosized alumina particles. J Appl Phys 2002;91:4568–72. https://doi.org/10.1063/1.1454184.

[31] Masoumi N, Sohrabi N, Behzadmehr A. A new model for calculating the effective viscosity of nanofluids. J Phys D Appl Phys 2009;42. https://doi.org/10.1088/0022-3727/42/5/055501.

[32] Ali AM, Angelino M, Rona A. Physically Consistent Implementation of the Mixture Model for Modelling Nanofluid Conjugate Heat Transfer in Minichannel Heat Sinks. Appl Sci 2022;12. https://doi.org/10.3390/app12147011.

[33] Kleinstreuer C, Feng Y. Erratum to: Experimental and theoretical studies of nanofluid thermal conductivity enhancement: a review. Nanoscale Res Lett 2011;6:27695. https://doi.org/10.1186/1556-276x-6-439.

[34] Gianluca Coccia, Sebastiano Tomassetti GDN. Thermal conductivity of nanofluids: A review of the existing correlations and a scaled semi-empirical equation. Renew Sustain Energy Rev 2021;151. https://doi.org/10.1016/j.rser.2021.111573.

[35] Junhao Li, Xilong Zhang, Bin Xu MY. Nanofluid research and applications: A review. Int Commun Heat Mass Transf 2021;127. https://doi.org/10.1016/j.icheatmasstransfer.2021.105543.

[36] Meriem I, Benchabi R. Contribution to the Thermal and Hydraulic Study of Forced Convection in Corrugated Configuration Using Nanofluids. J Nanofluids 2024;13:735–48. https://doi.org/10.1166/jon.2024.2166.

[37] Talari VK, Thamida SK, Srinivas T, Purohit BK. Optimization of Nanofluid Concentration for Energy Intensification in Corrugated Plate Type Heat Exchanger. J Nanofluids 2024;13:674–85. https://doi.org/10.1166/jon.2024.2161.

[38] Kurşun B. Thermal performance assessment of internal longitudinal fins with sinusoidal lateral surfaces in parabolic trough receiver tubes. Renew Energy 2019;140:816–27. https://doi.org/10.1016/j.renene.2019.03.106.

[39] Sudarmadji Sudarmadji* BS and S. Performance Evaluation Criterion of Nanofluid. Microfluid. Nanofluidics, 2012, p. 277–89.

[40] Alemam A, Yehya SA, Omer AS, Hamza A, Saeed M, Berrouk AS. Performance Comparison of Mini-Rectangular Fin Heat Sinks Using Different Coolants: Supercritical CO2, Water and Al2O3/H2O Nanofluid. Energies 2022;15. https://doi.org/10.3390/en15228734.

[41] Montazerifar F, Amidpour M, Abedi Z. Numerical investigation of turbulent nanofluid flow behavior in a multi-stream plate-fin heat exchanger with a novel design of fractal fins. Alexandria Eng J 2023;72:431–49. https://doi.org/10.1016/j.aej.2023.03.090.

[42] Mohammadzadeh AM, Jafari B, Hosseinzadeh K, Paikar E. Numerical investigation of segmental baffle design in shell and tube heat exchangers with varying inclination angles and spacing. Sci Rep 2025;15:1–20. https://doi.org/10.1038/s41598-025-87652-x.

[43] Buongiorno J. Convective Transport in Nanofluids. J Heat Transfer 2006;128:240–50. https://doi.org/10.1115/1.2150834.

[44] Khanafer K, Vafai K. International Journal of Heat and Mass Transfer A critical synthesis of thermophysical characteristics of nanofluids. Int J Heat Mass Transf 2011;54:4410–28. https://doi.org/10.1016/j.ijheatmasstransfer.2011.04.048.

[45] Shah, Ramesh & Sekulić D. FUNDAMENTALS OF HEAT EXCHANGER DESIGN. John Wiley & Sons, Inc., Hoboken, New Jersey; 2007. https://doi.org/10.1002/9780470172605.fmatter.

[46] Hassaan A. An investigation for the performance of the using of nanofluids in shell and tube heat exchanger. Int J Therm Sci 2022;177. https://doi.org/10.1016/j.ijthermalsci.2022.107569.

[47] Göktepe S, Atalik K, Ertürk H. Comparison of single and two-phase models for nanofluid convection at the entrance of a uniformly heated tube. Int J Therm Sci 2014;80:83–92. https://doi.org/10.1016/j.ijthermalsci.2014.01.014.

Supplementary Files

This is a list of supplementary files associated with this preprint. Click to download.

- GraphicalAbstract.tif